Silicon Electrodeposition in Water-Soluble KF-KCl Molten Salt: Investigations on the Reduction of Si(IV) Ions

AUTHOR(S):

Maeda, Kazuma; Yasuda, Kouji; Nohira, Toshiyuki; Hagiwara, Rika; Homma, Takayuki

CITATION:

Maeda, Kazuma ...[et al]. Silicon Electrodeposition in Water-Soluble KF-KCl Molten Salt: Investigations on the Reduction of Si(IV) Ions. Journal of the Electrochemical Society 2015, 162(9): D444-D448

ISSUE DATE:

2015-06-09

URL:

http://hdl.handle.net/2433/201557

Title:

Silicon Electrodeposition in Water-soluble KF–KCl Molten Salt: Investigations on the Reduction of Si(IV) Ions

Authors:

Kazuma MAEDA,[a] Kouji YASUDA,[a,b,*] Toshiyuki NOHIRA,[a,*]

Rika HAGIWARA[a] and Takayuki HOMMA[c]

Affiliation:

[a]Department of Fundamental Energy Science, Graduate School of Energy Science, Kyoto University, Yoshida-hommachi, Sakyo-ku, Kyoto 606-8501, Japan.

[b]Environment, Safety and Health Organization, Kyoto University, Yoshida-hommachi, Sakyo-ku, Kyoto 606-8501, Japan.

[c]Faculty of Science and Engineering, Waseda University, 3-4-1 Okubo, Shinjuku-ku, Tokyo 169-8555, Japan.

***Corresponding Authors:**

yasuda.kouji.3v@kyoto-u.ac.jp (K. Yasuda)

nohira.toshiyuki.8r@kyoto-u.ac.jp (T. Nohira)

Tel.: +81-75-753-4817; Fax: +81-75-753-5906.

Abstract

A new method for electroplating Si using a water-soluble KF–KCl molten salt electrolyte and high-purity gaseous $SiCl_4$ has been proposed. To gain a fundamental understanding of the process, the electrodeposition of Si from Si(IV) complex ions on a Ag electrode in a molten KF–KCl–K_2SiF_6 system was investigated by cyclic voltammetry at 923 K. The reduction of Si(IV) ions to metallic Si was observed as a single 4-electron wave, which is explained by an E_qE_r (quasireversible-reversible electron transfer reactions) mechanism. The diffusion coefficient of the Si(IV) ions in the electrolyte was determined to be 3.2×10^{-5} cm^2 s^{-1} at 923 K by chronoamperometry.

Keywords:

Molten salt; silicon; electrodeposition; fluoride-chloride

1. Introduction

Photovoltaic (PV) power generation has attracted much interest as a method for harvesting renewable energy. Solar cells are generally categorized into three types, namely Si, compound, and organic solar cells. Among these, the most prevalent type of solar cell is the crystalline Si solar cell, which accounted for 90.1% of the total production in 2013 [1]. With the widespread use of Si solar cells, the high-purity polycrystalline Si production capacity of the major producers has reached 233,800 tons in 2013 [2], which is approximately fifteen times larger than the production capacity a decade ago. Until the late 2000s, high-purity Si for the fabrication of crystalline Si solar cells, known as solar-grade Si (SOG-Si, 6N purity), was predominantly supplied from off-grade portions (such as tops, bottoms, and edges of monocrystalline Si ingots) of semiconductor-grade Si (SEG-Si, 11N–12N purity), manufactured by the Siemens process [3,4]. However, the situation has changed drastically in recent years, and currently over 90% of high-purity polycrystalline Si is produced exclusively for solar cell fabrication, owing to the rapid growth of the PV industry.

The current fabrication process for crystalline Si solar cells has several drawbacks from the points of view of energy efficiency and yield. These drawbacks mainly result from the low productivity and yield of the Siemens process, owing to the considerable kerf loss in the Si slicing process. One of the alternative methods for producing polycrystalline Si solar cells is the direct formation of Si films on cell substrates. The advantage of this method is that Si can be efficiently used by avoiding the slicing step.

Electrodeposition is a good technique for the formation of Si films. According to several papers in the literature, only amorphous Si is electrodeposited in organic solvents and crystalline Si cannot be electrodeposited [5,6]. The electrodeposition of amorphous

Si has also been reported in ionic liquid media [7,8]. On the other hand, the electrodeposition of crystalline Si has been reported in high-temperature molten salts since the 1970's [9,10]. In previous studies, fluoride, chloride, and fluoride-chloride molten salts have been used as electrolytes for the electrodeposition of Si [11–22]. Elwell *et al*. obtained a relatively compact and smooth Si layer in molten LiF–NaF–KF at 1018 K [11,12]. Deposits with acceptable quality have also been obtained from binary LiF–KF systems [13]. The mechanism for the electrochemical reduction of Si(IV) ions to metallic Si has been reported to be different in different molten salts. For example, the reduction of Si(IV) ions has been reported to proceed in one-step reaction in the LiF–NaF–KF system [14], whereas it proceeds in two-step reaction in LiF–KF [15,16] and NaF–KF [17]. Lepinay *et al*. reported that the reduction of Si(IV) ions in a ternary LiF–NaF–KF system proceeds in two-step reaction, coupled with a proportionation reaction [18]. In the case of chloride salts (e.g., NaCl–KCl system), the electrodeposition of Si proceeds in two-step reduction mechanism [19]. However, Si deposits of good quality have not been obtained in this the chloride media [19,20]. Kuznetsova *et al*. concluded that the reduction of Si(IV) ions proceeds in two-step in molten NaCl–KCl–NaF [21], which is a chloride-fluoride melt. They also determined the diffusion coefficients of the Si(IV) and Si(II) ions in this medium [21]. In addition, the electrodeposition of Si was reported in molten KF–KCl–K_2SiF_6 after dissolving SiO_2 in the melt [22]. However, the deposit contained only 20–50 wt% of powder-like Si. Moreover, the addition of SiO_2 requires the elimination of O^{2-} ions from the melt, which is practically possible only by using a carbon anode in molten fluorides. This inevitably causes carbon contamination in the Si deposits, owing to the formation of CO_3^{2-} ions. In summary, the use of fluoride-based

molten salts, such as LiF–KF and LiF–NaF–KF, is effective for obtaining compact and smooth Si films, and the use of SiO_2 as a Si ion source should be avoided.

However, a major problem in the previous investigations employing fluoride-based molten salts was the removal of the salt adhered to the deposited Si [16,22], because the solubilities of LiF and NaF in water are very low [23]. Another inherent problem is the lack of availability of high-purity and low-cost Si sources. Conventionally, either K_2SiF_6 or anodic dissolution of a Si rod has been utilized for supplying Si ions. However, it is difficult to prepare K_2SiF_6 and Si rods of solar grade purity at low costs.

In this study, we propose a new electrodeposition process for Si with KF–KCl as the molten salt electrolyte and high-purity gaseous $SiCl_4$ used as the Si source. A schematic illustration of the process is shown in Fig. 1. The KF–KCl system is selected for the following reasons. First, as described in the previous paragraph, a fluoride-based molten salt is a reasonable choice for obtaining compact and smooth Si films. Among alkali and alkaline earth fluorides, KF has exceptionally high solubility in water (101.6 g 100 g-H_2O^{-1}, cf. LiF; 0.13 g 100 g-H_2O^{-1}, NaF; 0.15 g 100 g-H_2O^{-1}, MgF_2; 0.13 g 100 g-H_2O^{-1}, CaF_2; 0.0016 g 100 g-H_2O^{-1}) [23]. The use of a single KF molten salt is, however, rather difficult, owing to the high melting point of KF (1131 K). Since KCl also has high solubility in water, electrolysis can be conducted at low temperatures and the adhered salt can be removed easily by washing with water, if a KF–KCl binary system is used (melting point = 878 K at the eutectic composition [24]). Although LiCl, NaCl, $MgCl_2$, and $CaCl_2$ also have high solubilities to water, the addition of any of them to KF inevitably results in the formation of a water-insoluble fluoride salt. High-purity $SiCl_4$ is selected as a Si source because it can be produced at low cost. When gaseous $SiCl_4$ is

introduced into molten KF–KCl, $SiCl_4$ chemically dissolves in the melt to form SiF_6^{2-} (or $SiF_xCl_y^{(x+y-4)-}$) ions (Eq. 1)

$$\text{Dissolution:} \quad SiCl_4\,(g) + 6\,F^- \rightarrow SiF_6^{2-} + 4\,Cl^- \tag{1}$$

The resultant molten salt is identical to the molten KF–KCl–K_2SiF_6 system. In this system, the electrochemical reactions at the cathode and anode would be Si deposition and Cl_2 gas evolution, respectively, as shown in Eqs. 2-3.

$$\text{Cathode:} \quad SiF_6^{2-} + 4\,e^- \rightarrow Si\,(s) + 6\,F^- \tag{2}$$

$$\text{Anode:} \quad 4\,Cl^- \rightarrow 2\,Cl_2\,(g) + 4\,e^- \tag{3}$$

The total reaction may be given by Eq. 4.

$$\text{Total:} \quad SiCl_4\,(g) \rightarrow Si\,(s) + 2\,Cl_2 \tag{4}$$

Therefore, Si can be electrodeposited without change in the composition of the molten salt. Moreover, the evolved Cl_2 gas can be reused for the production of gaseous $SiCl_4$.

As a first step, in the present work, we have focused on obtaining fundamental electrochemical data on the molten KF–KCl–K_2SiF_6 system at 923 K. The reversibility of the electrochemical reaction, diffusion coefficient of Si(IV) ions, transfer coefficient, and number of electrons transferred in the rate-determining step have been studied by cyclic voltammetry at various K_2SiF_6 concentrations and scan rates.

2. Experimental

A schematic drawing of the experimental apparatus is shown in Fig. 2. Reagent-grade KF (Wako Pure Chemical Co. Ltd., >99.0%) and KCl (Wako Pure Chemical Co. Ltd., >99.5%) were mixed to achieve the eutectic composition (molar ratio of KF/KCl = 45:55, melting point = 878 K [24]) and loaded in a graphite crucible (Toyo Tanso Co. Ltd., outer diameter: 90 mm, inner diameter: 80 mm, and height: 120 mm). The mixture in the crucible was first dried under vacuum at 453 K for 72 h to remove residual moisture. The crucible was placed at the bottom of a quartz vessel in an air-tight Kanthal container and further dried under vacuum at 673 K for 24 h. The electrochemical experiments were conducted in a dry Ar atmosphere at 923 K. After blank measurements, K_2SiF_6 (Wako Pure Chemical Co., Ltd., >95%) was added to the melt.

Electrochemical measurements and galvanostatic electrolysis were conducted using a three-electrode electrochemical measurement system (Princeton Applied Research, VersaSTAT4). The working electrodes included a Ag plate (Nilaco Corp., thickness: 0.1 mm, 99.98%) and Ag flag electrode (Nilaco Corp., thickness: 0.1 mm, 99.98%). As shown in Fig. 3, the Ag flag electrode consisted of a Ag disk (diameter: 2.0 or 5.0 mm, thickness: 0.1 mm), to which a thin Ag lead wire was welded (Nilaco Corp., diameter: 0.1 mm, 99.98%). A glassy carbon rod (Tokai Carbon Co., Ltd., diameter: 5.0 mm) was used as the counter electrode, while a Pt wire (Nilaco corp., >99.98%, diameter: 1.0 mm) was employed as a quasi-reference electrode. The potential of the reference electrode was calibrated with reference to a dynamic K^+/K potential which was prepared by the electrodeposition of K metal on a Ag wire. The temperature of the melt was measured using a type K thermocouple which was inserted into an insulating alumina tube (Nikkato

Corp., SSA-S grade, outer diameter: 6 mm, inner diameter: 4 mm, and length: 500 mm). The thermocouple was set above the molten salt except during the measurement of the bath temperature in order to avoid the corrosion. The electrolyzed samples on the Ag plates were washed with distilled water at 333 K for 24 h to remove salt adhered on the deposits, and then dried under vacuum at room temperature for 12 h. The cross-sections of the samples were then observed using a scanning electron microscope (SEM; Keyence Corp., VE-8800). For these observations, the samples were embedded in acrylic resin and polished with emery paper and a buffing compound. After polishing, the samples were coated with Au using an ion sputtering apparatus (Hitachi, Ltd., E-1010) to obtain a conductive coating. The deposits were also characterized by energy dispersive X-ray spectroscopy (EDX; AMETEK Co. Ltd., EDAX Genesis APEX2), X-ray diffraction (XRD; Rigaku Corp., Ultima IV, Cu-Kα line), and Raman spectroscopy (Tokyo Instruments Corp., Nanofinder30).

3. Results and Discussion

3.1 Cyclic voltammetry

For cyclic voltammetry, the Ag flag electrode was used because it has a reproducible electrode area and is suitable for quantitative analysis of the reaction. Figure 4(a) shows the cyclic voltammograms for the Ag flag electrode in molten KF–KCl–K_2SiF_6 with various K_2SiF_6 concentrations (blank, 0.50, 2.0, 3.5, and 5.0 mol%) at 923 K. The cyclic voltammograms were measured at a scan rate of 0.50 V s^{-1}. In the case of the blank measurements (without addition of K_2SiF_6; dotted line), the cathodic current gradually increases at around 0.2 V vs. K^+/K in the negative sweep and a large current is observed at more negative potential than 0 V. Since Ag forms no alloys or intermetallic

compounds with K and Si at 923 K [25,26], the gradual increase in current from 0.2 V and the sharp increase from 0 V are attributed to the formation of K metal fog and the deposition of liquid K metal (Eq. 5), respectively.

$$K^+ + e^- \rightarrow K\ (l) \tag{5}$$

When the potential sweep direction is reversed, anodic dissolution of the deposited K metal is observed. The potential at zero current in the linear region (Point A) during the positive sweep is equivalent to the redox potential of K^+/K observed for the K metal on a Ag wire. All the potentials are calibrated and reported with reference to this K^+/K potential.

Cyclic voltammograms of a Ag flag electrode recorded after the addition of various amounts of K_2SiF_6 are also shown in Fig. 4(a). In the negative sweep direction, a single cathodic wave starting around 0.75 V is observed in each K_2SiF_6 concentration. After the reversal of the sweep direction, two anodic waves, a shoulder and a peak, are observed from 0.75 V. Since both the cathodic and anodic peak current densities increase with the K_2SiF_6 concentration, the cathodic and anodic peaks are likely related to the deposition and dissolution of Si, respectively. Here, it should be noted that the appearance of the oxidation shoulder is more obvious at high scan rates. This shape of the voltammograms suggests that the reduction proceeds with a multiple-electron reaction of an E_qE_r (quasireversible-reversible electron transfer reactions) mechanism [27].

Figure 4(b) shows the cyclic voltammogram for a glassy carbon electrode at a scan rate of 0.50 V s^{-1} in the positive potential region in the KF–KCl molten salt without the

addition of K_2SiF_6. A sharp increase of current corresponding to Cl_2 gas evolution was observed at approximately 3.5 V on the positive sweep.

$$2\ Cl^- \rightarrow Cl_2 + 2\ e^- \quad (6)$$

From these voltammetric results, electrochemical window of the KF–KCl melt was estimated to be 3.5 V at 923 K. This value agrees well with that calculated from the standard Gibbs energy of formation of KCl(*l*), 3.54 V [28], assuming that the activity of each anion follows the Raoult's law.

3.2 Analysis of the deposition process

To confirm that the redox peaks observed in the cyclic voltammograms correspond to the deposition and dissolution of Si, galvanostatic electrolysis was conducted using a Ag plate electrode at a current density of −60 mA cm^{-2} for 60 min in molten KF–KCl–K_2SiF_6 (2.0 mol%) at 923 K. Figure 5 (a), (b), and (c) show a cross-sectional SEM image, XRD pattern, and Raman spectrum, respectively, of the sample obtained by the galvanostatic electrolysis and subsequent washing treatment. The SEM image in Fig. 5(a) confirms that an adherent, compact, and smooth film with a thickness of 50 μm is electrodeposited on the Ag substrate. No other elements, besides Si, are observed in the EDX spectra. All the peaks in the XRD pattern in Fig. 5(b) are attributable to the Si deposits and Ag substrate. Further, the Raman spectrum in Fig. 5(c) shows a peak corresponding to crystalline Si (517 cm^{-1}), whereas no peak corresponding to amorphous Si (480 cm^{-1}) is observed. The current efficiency calculated from the sample weight and electric charge was 93%. From these results, it is concluded that the film deposited on the

Ag plate is composed of crystalline Si, and that the cathodic wave in the cyclic voltammograms in KF–KCl–K_2SiF_6 are assigned to a single 4-electron wave from Si(IV) to Si(0).

3.3 Electrochemical study of the reduction of Si(IV) ions

The electrochemical reduction process of Si(IV) ions to metallic Si (Si(0)) in the KF–KCl–K_2SiF_6 molten salt electrolyte was studied by cyclic voltammetry at 923 K. Figure 6 shows the cyclic voltammograms of a Ag flag electrode (diameter: 5 mm) obtained at different scan rates (0.05, 0.2, 0.5, and 2 V s^{-1}). The cathodic peak potentials in the cyclic voltammograms shift to negative values with increase in the scan rate. For example, the cathodic peak potential is 0.73 V at a scan rate of 0.05 V s^{-1}, whereas it is 0.56 V at a scan rate of 2 V s^{-1}. This shift indicates that the electrochemical reduction is either an irreversible process or a quasireversible process.

To clarify whether the electrochemical reaction is irreversible or quasireversible, the relationship between scan rate and peak current was investigated. The cathodic peak current, I_{cp}, for the irreversible process is given by Eq. 7, regardless of whether the reaction product is soluble or not [29].

$$I_{cp} = -0.496nFAc_o\,(\alpha n_\alpha D_o F v / RT)^{1/2} \qquad (7)$$

In the above equation, n is the number of electrons transferred, F is the Faraday constant, A is the electrode area, c_o is the concentration of ions in the electrolyte, α is the transfer coefficient, n_α is the n value of the rate-determining step, D_o is the diffusion coefficient of the ions, v is the scan rate, R is the universal gas constant, and T is the absolute

temperature. From Eq. 7, it is evident that the cathodic current density ($i_{cp} = I_{cp}/A$) is proportional to the square root of the scan rate. On the other hand, i_{cp} is not proportional to $v^{1/2}$ for a quasireversible process.

The value of i_{cp} is plotted against $v^{1/2}$ in Fig. 7 for the cyclic voltammograms obtained in KF–KCl–K_2SiF_6 (0.10 and 0.40 mol%) electrolytes. In the measurements, i_{cp} is evaluated by subtracting the background current at the peak potential obtained in the melt without K_2SiF_6. Further, since the actual potential sweep rate becomes smaller at large currents owing to the IR drops in the electrolyte, two types of measures were taken. One is the in-situ IR compensation using the electrochemical measurement system. The compensation ratio was set around 80% which was the highest value in the range without bringing potential instability. The other is the use of an electrode with a diameter of 2 mm in the case of the electrolyte containing 0.40 mol% K_2SiF_6 to reduce the impact of IR drop. As seen in Fig. 7, i_{cp} is not proportional to $v^{1/2}$ at both electrolyte concentrations, and the approximated straight lines do not converge to the origin. Thus, the electrochemical reaction is concluded to be a quasireversible process. Taking into consideration the shape of the voltammograms shown in Fig. 4(a), the electrochemical reduction of Si(IV) ions to the metallic state is best explained by an E_qE_r mechanism. It should be noted that this two-step E_qE_r mechanism could be observed as a single wave in voltammetry [27]. In previous studies, both the one-step (a single wave in voltammetry) and two-step (two waves in voltammetry) mechanisms have been reported in fluoride molten salts [14,18], whereas only the two-step mechanism has been reported in chloride molten salts [19]. The reduction mechanism in mixed KF–KCl systems would be affected by the concentration of chloride ions.

Further, the diffusion coefficient of the Si(IV) ions was evaluated from chronoamperometry. For the evaluation of the quasireversible system, the potential was set in the mass-transfer-limited region. Namely, 0.36 V, 0.46 V and 0.56 V were selected because they were more negative than the peak potential of Si deposition for the cyclic voltammogram at a scan rate of 0.5 V s^{-1} (0.63 V). When the rate-determining step is a diffusion of ions, the current-time response follows a Cottrell equation. The current, *I*, is proportional to the reciprocal of square root of time, *t*, in the measurements under constant concentration conditions [30].

$$I = -\frac{nFAD_{\mathrm{O}}^{1/2}c_{\mathrm{O}}}{\pi^{1/2}t^{1/2}} \tag{8}$$

The values of D_o can then be determined from the slope of the graph which plots current value against reciprocal of square root of time.

Figure 8(a) shows a chronoamperogram for a Ag flag electrode in molten KF–KCl–K_2SiF_6 (0.10 mol%) at 923 K. The cathodic current density approaches to −25 mA cm^{-2} at 0.46 V and 0.56 V, while it is larger at 0.36 V. The large value suggests that the current for the formation of K metal fog is superimposed on that for the deposition of Si. In the evaluation of D_o from the Cottrell equation, the observed current is identical even at different potentials. Then, the evaluation of D_o was carried out based on the results of 0.46 V and 0.56 V.

Figure 8(b) shows the relationship between the current density and the reciprocal of square root of time. They have proportional relations in the small $t^{-1/2}$ range, but deviate in the large $t^{-1/2}$ range at 0.46 V and 0.56 V. The deviation suggests that the reaction is not limited only by mass-transfer. Since the proportional relationship is observed for

larger $t^{-1/2}$ range at 0.46 V, D_o is calculated from the data at 0.46 V. The volume concentration of ions in the electrolyte, c_o, is calculated using the density of the KF–KCl melt (KF:KCl = 50:50 mol%, ρ = 1.7595 g cm^{-3} at 923 K), which is estimated by extrapolating the reported data in the temperature range of 1050–1250 K [31]. The diffusion coefficient of Si(IV) ions in KF–KCl–K_2SiF_6 (0.10 mol%) at 923 K is calculated to be 3.2×10^{-5} cm^2 s^{-1}. The diffusion coefficient value obtained in this study is close to the value of 5.4×10^{-5} cm^2 s^{-1} in molten KF–KCl at 933 K obtained by Boiko *et al.* using chronoamperometry [32].

4. Conclusion

The electrodeposition of Si was investigated in a molten KF–KCl–K_2SiF_6 electrolyte system at 923 K. The deposition of crystalline Si on a Ag electrode by electrolysis was confirmed by XRD and Raman spectroscopy. Further, cyclic voltammetry and chronoamperometry of a Ag electrode was conducted to study the electrochemical behavior of Si(IV) complexes. The cathodic peak potential in the cyclic voltammograms shifted to negative values with increase in the scan rate, whereas the cathodic peak current density does not change proportionally to the square root of the scan rate. These results indicate that the reduction of Si(IV) to Si(0) is a quasireversible electrochemical reaction, which is best explained by an E_qE_r mechanism. Further, the diffusion coefficient of the Si(IV) complexes was determined from chronoamperometry to be 3.2×10^{-5} cm^2 s^{-1} in the KF–KCl–K_2SiF_6 (0.10 mol%) melt at 923 K.

Nomenclature

Character	Meaning	Unit
α	Transfer coefficient	—
A	Electrode area	cm^2
c_o	Concentration of ions in electrolyte	mol cm^{-3}
D_o	Diffusion coefficient of ions	cm^2 s^{-1}
F	Faraday constant	C mol^{-1}
i_{cp}	Cathodic peak current density	A cm^{-2}
I_{cp}	Cathodic peak current	A
k°	Standard rate constant	cm s^{-1}
n	Number of electrons transferred in the reaction	—
n_α	Number of electrons transferred in the rate-determining reaction	—
R	Gas constant	J K^{-1} mol^{-1}
T	Absolute temperature	K
t	Time	s
v	Scan rate	V s^{-1}

Acknowledgments

This study was partly supported by the Core Research for Evolutionary Science and Technology (CREST) from the Japan Science and Technology Agency (JST).

References

1. *Rare Metal News*, Arumu Publ. Co., on August 24, 2014. [in Japanese]
2. *Rare Metal News*, Arumu Publ. Co., on Aplil 1, 2014. [in Japanese]
3. H. Schweickert, K. Reuschel and H. Gutsche: U.S. Patent 3,011,877 (1961).
4. H. Gutsche: U.S. Patent 3,042,494 (1962).
5. Y. Takeda, R. Kanno and O. Yamamoto, *J. Electrochem. Soc.*, **128**, 1221 (1981).
6. M. Bechelany, J. Elias, P. Brodard, J. Michler and L. Philippe, *Thin Solid Films*, **520**, 1895 (2012).
7. S. Z. E. Abedin, N. Borissenko and F. Endres, *Electrochem. Commun.*, **6**, 510 (2004).
8. Y. Nishimura, Y. Fukunaka, T. Nishida, T. Nohira and R. Hagiwara, *Electrochem. Solid-State Lett.*, **11**, D75 (2008).
9. D. Elwell, *J. Crystal Growth*, **52**, 741 (1981).
10. J. Xu and G. M. Haarberg, *High Temp. Mater. Proc.*, **32**, 97 (2013).
11. G. M. Rao, D. Elwell and R. S. Feigelson, *J. Electrochem. Soc.*, **127**, 1940 (1980).
12. D. Elwell and R. S. Feigelson, *Sol. Energ. Mat.*, **6**, 123 (1982).
13. U. Cohen and R. A. Huggins, *J. Electrochem. Soc.*, **123**, 381 (1976).
14. D. Elwell and G. M. Rao, *Electrochim. Acta*, **27**, 673 (1982).
15. K. S. Osen, A. M. Martinez, S. Rolseth, H. Gudbrandsen, M. Juel and G. M. Haarberg, *ECS Trans.*, **33**, 429 (2010).
16. G. M. Haarberg, L. Famiyeh, A. M. Martinez and K. S. Osen, *Electrochim. Acta*, **100**, 226 (2013).
17. A. L. Bieber, L. Massot, M. Gibilaro, L. Cassayre, P. Taxil and P. Chamelot, *Electrochim. Acta.*, **62**, 282 (2012).

18. J. D. Lepinay, J. Bouteillon, S. Traore, D. Renaud and M. J. Barbier, *J. App. Electrochem.*, **17**, 294 (1987).
19. S. V. Devyatkin, *J. Mining Metallurgy*, **39B**, 303 (2003).
20. R. Boen and J. Bouteillon, *J. App. Electrochem.*, **13**, 277 (1983).
21. S. V. Kuznetsova, V. S. Dolmatov and S. A. Kuznetsov, *Russ. J. Electrochem.* **45**, 797 (2009).
22. A. A. Andriiko, E. V. Panov, O. I. Boiko, B. V. Yakovlev and O. Y. Borovik, *Russ. J. Electrochem.*, **33**, 1343 (1997).
23. R. Kubo, S. Nagakura, H. Iguchi and H. Ezawa, *Rikagaku Jiten, 4th Edition*, Iwanami Shoten, Tokyo (1987).
24. L. P. Cook and H. F. McMurdie, *Phase Diagrams for Ceramists vol. VII*, p. 509, The American Ceramic Society Inc., Columbus (1989).
25. A. D. Pelton, *Bulletin of Alloy Phase Diagrams*, **7**, 223 (1986).
26. R. W. Olesinski, A. B. Gokhale and G. J. Abbaschian, *Bulletin of Alloy Phase Diagrams.*, **10**, 635 (1989).
27. A. J. Bard and L. R. Faulkner, *Electrochemical Methods: Fundamentals and Applications, 2nd Edition*, John Wiley& Sons, New York, p. 510 (2001).
28. M. W. Chase, JANAF Thermochemical Tables, Third Edition Part II, 1022 (1985).
29. R. S. Nicholson and I. Shain, *Anal. Chem.*, **36**, 706 (1964).
30. F. G. Cottrell, *Z. Physik. Chem*, **42**, 385 (1902).
31. G. J. Janz, *J. Phys. Chem. Ref. Date*, **17**, 1 (1988).
32. O. I. Boiko, Y. K. Delimarskii and R. V. Chernov, *Ukr. Khim. Zh.*, **51**, 385 (1985).

Figures captions

Fig. 1 Schematic illustration for the principle of electroplating process of Si in KF–KCl molten salt.

Fig. 2 Schematic drawing of the experimental apparatus. (A) Ag plate electrode, (B) Ag flag electrode, (C) glassy carbon electrode, (D) Pt electrode, (E) thermocouple, (F) quartz inner vessel, (G) graphite crucible and (H) molten KF–KCl.

Fig. 3 A photograph of the Ag flag electrode.

Fig. 4 Cyclic voltammograms for (a) a Ag flag electrode and (b) a glassy carbon electrode in molten KF–KCl–K_2SiF_6 (blank, 0.50, 2.0, 3.5 and 5.0 mol%) at 923 K. Scan rate: 0.50 V s^{-1}.

Fig. 5 (a) A Cross-sectional SEM image, (b) XRD pattern and (c) Raman spectrum of the sample obtained by galvanostatic electrolysis of a Ag plate electrode at −60 mA cm^{-2} for 60 min in molten KF–KCl–K_2SiF_6 (2.0 mol%) at 923 K.

Fig. 6 Cyclic voltammograms for a Ag electrode in molten KF–KCl–K_2SiF_6 (0.10 mol%) at various scan rates at 923 K.

Fig. 7 Dependence of cathodic peak current density on scan rate. The cyclic voltammetry was carried out in molten KF–KCl–K_2SiF_6 (0.10 and 0.40 mol%) at 923 K.

Fig. 8 (a) Chronoamperograms for a Ag flag electrode, and (b) relationship of the current density and the reciprocal of square root of time at 0.36, 0.46 and 0.56 V vs. K^+/K in molten KF–KCl–K_2SiF_6 (0.10 mol%) at 923 K.

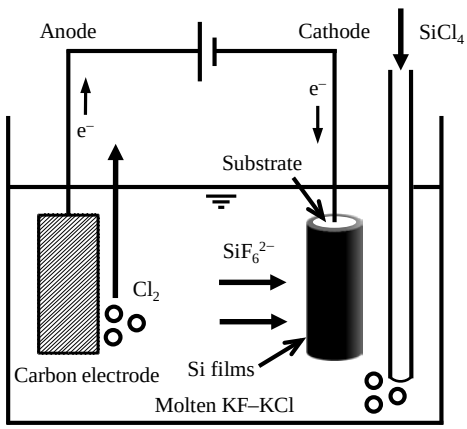

Fig. 1 Schematic illustration for the principle of electroplating process of Si in KF–KCl molten salt.

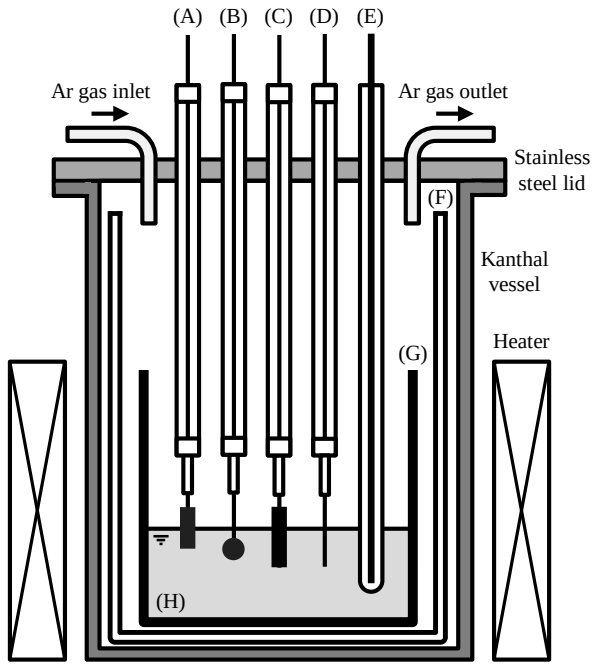

Fig. 2 Schematic drawing of the experimental apparatus. (A) Ag plate electrode, (B) Ag flag electrode, (C) glassy carbon electrode, (D) Pt electrode, (E) thermocouple, (F) quartz inner vessel, (G) graphite crucible and (H) molten KF–KCl.

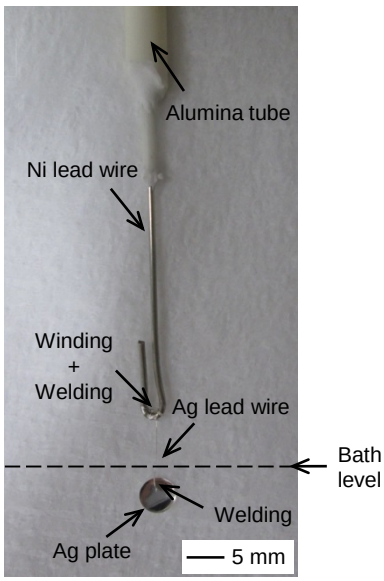

Fig. 3 A photograph of the Ag flag electrode.

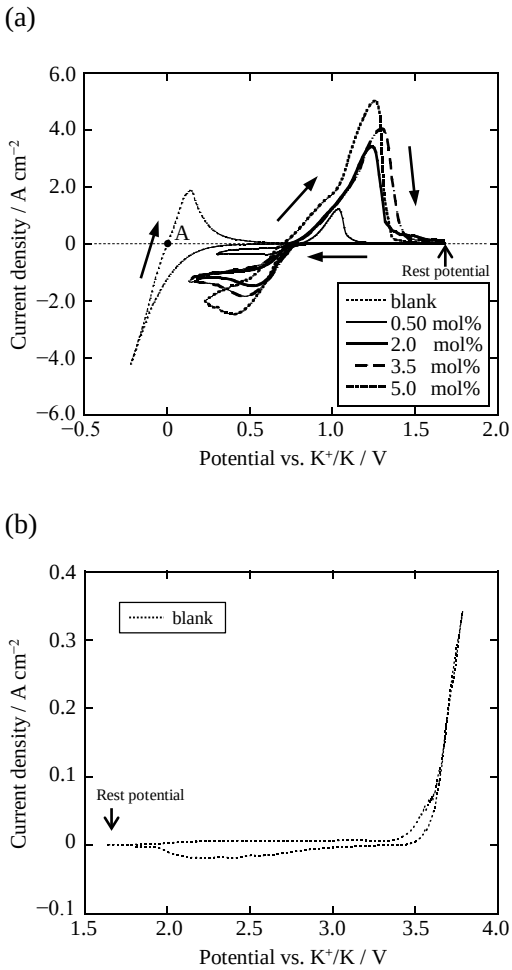

Fig. 4 Cyclic voltammgrams for (a) a Ag flag electrode and (b) a glassy carbon electrode in molten KF–KCl–K_2SiF_6 (blank, 0.50, 2.0, 3.5 and 5.0 mol%) at 923 K. Scan rate: 0.50 V s^{-1}.

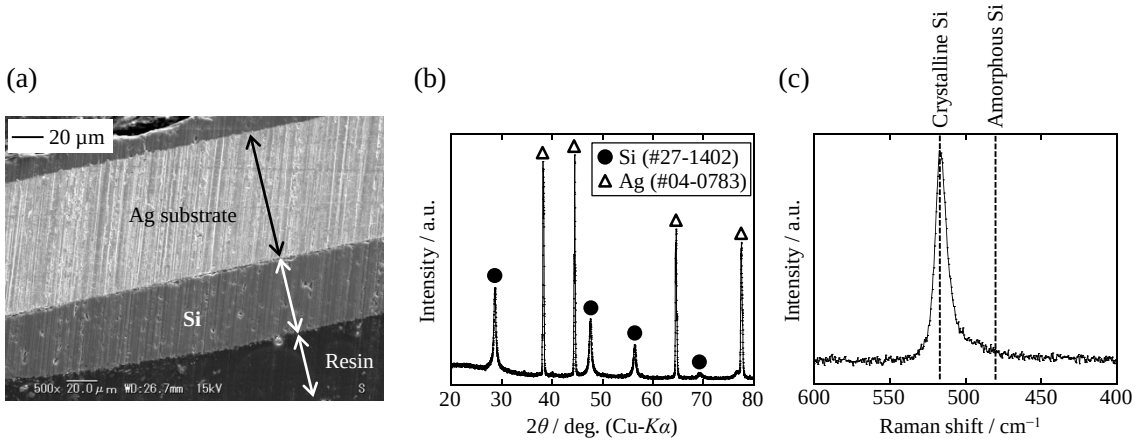

Fig. 5 (a) A Cross-sectional SEM image, (b) XRD pattern and (c) Raman spectrum of the sample obtained by galvanostatic electrolysis of a Ag plate electrode at −60 mA cm^{-2} for 60 min in molten KF–KCl–K_2SiF_6 (2.0 mol%) at 923 K.

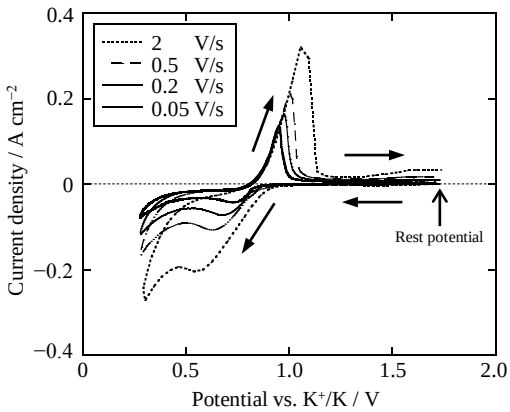

Fig. 6 Cyclic voltammograms for a Ag electrode in molten KF–KCl–K_2SiF_6 (0.10 mol%) at various scan rates at 923 K.

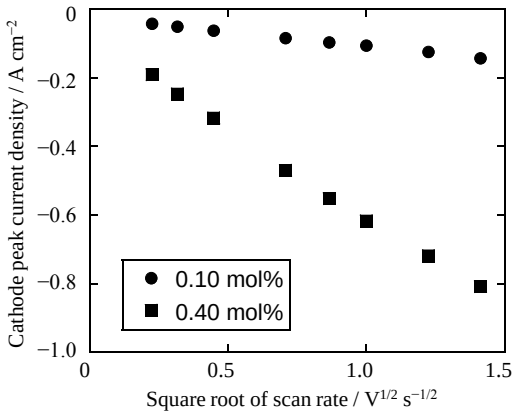

Fig. 7 Dependence of cathodic peak current density on scan rate. The cyclic voltammetry was carried out in molten KF–KCl–K_2SiF_6 (0.10 and 0.40 mol%) at 923 K.

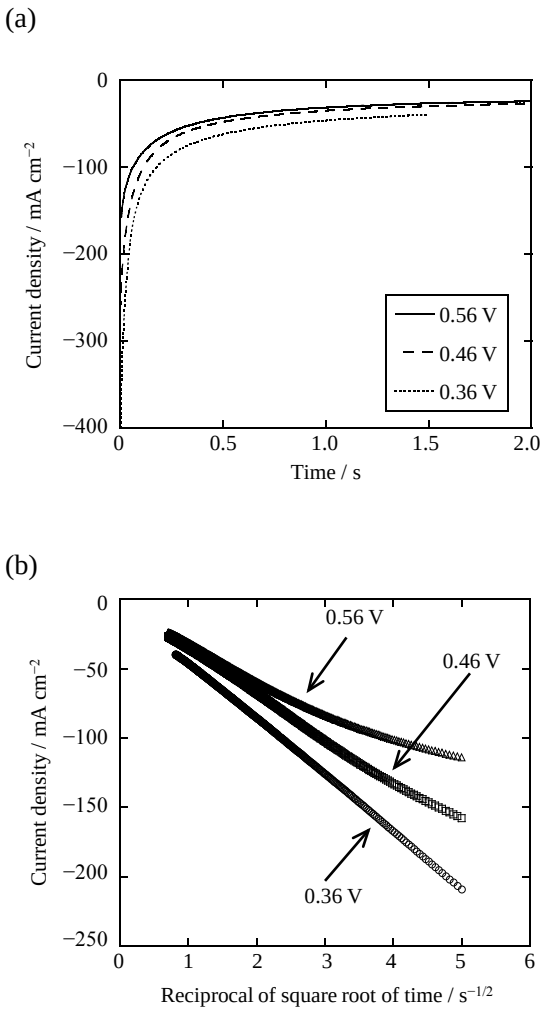

Fig. 8 (a) Chronoamperograms for a Ag flag electrode, and (b) relationship of the current density and the reciprocal of square root of time at 0.36, 0.46 and 0.56 V vs. K^+/K in molten KF–KCl–K_2SiF_6 (0.10 mol%) at 923 K.